Chen Wan-Ting (Orcid ID: 0000-0003-2294-1461)

Polymer grafted aramid nanofiber reinforces immiscible waste polypropylene/poly (ethylene terephthalate)

Shawn Martey,[1] Andrew Traywick,[2] Jesse C. Kelly,[2] Margaret J. Sobkowicz, [1] and Wan-Ting Chen [1, *]

[1] Department of Plastics Engineering University of Massachusetts Lowell, Massachusetts, USA

[2]Luna Labs USA, Charlottesville, Virginia, USA

Corresponding Authors: Prof. Wan-Ting (Grace) Chen, Email: GraceWanTing_Chen@uml.edu

Abstract

Polypropylene (PP) and Poly(ethylene terephthalate) (PET) are plastics commonly used for packaging because of their excellent barrier and mechanical properties. The properties of these plastics are often diminished after mechanical recycling, inevitably causing down-cycling. This problem is exacerbated when different kinds of polymers mix. Aramid nanofibers have the potential to improve the mechanical properties of polymers due to their excellent mechanical properties but their poor dispersion in polymers is a challenge. Grafting polymers onto nanofibers can help address this challenge. In this work, different loading levels (1%, 2% and 5%) of polymer grafted aramid nanofibers (ANF) are blended with waste PP/PET (90/10), simulating a PP waste stream containing traces of PET contaminants. Scanning electronic microscopy (SEM), rheology, and differential scanning calorimetry (DSC) results show the affinity of PP functionalized aramid nanofibers (PP_ANF) towards the PP matrix. At 1 wt.% of the nanofiber, the size of the PET droplets in the PP matrix of the PP_ANF blend range from 0.2-2.0 μm while that of unmodified ANF and PET_ANF blends are in the range of 0.1-6.2 and 0.5-7.4 μm respectively. In summary,

This is the author manuscript accepted for publication and has undergone full peer review but has not been through the copyediting, typesetting, pagination and proofreading process, which may lead to differences between this version and the Version of Record. Please cite this article as doi: 10.1002/app.54534

polymer grafted ANFs have the tendency of improving properties of its like polymers due to similarity in the grafting polymer and the polymer matrix.

Keywords: aramid nanofibers, polypropylene; poly(ethylene terephthalate), polymer blend, mechanical recycling, reinforcement

1. Introduction

Plastics are an indispensable part of our daily lives. They have been used for packaging, electronic, and automotive components, and healthcare instruments due to their low cost, durability, and ease of processing. At end-of-life, these plastics become post-consumer waste. This highly heterogeneous post-consumer plastic waste ends up in landfills or incinerated.[1,2]

Ineffective sorting of plastic waste is one of the major challenges of mechanical recycling of plastics, resulting in products made of mixed plastics waste. Because most polymer blends are immiscible due to their low entropy of mixing, poor interfacial adhesion is usually found in mixed plastic waste, leading to poor properties of mechanically recycled plastics.[3] Several compatibilization strategies have been studied to address this shortcoming. This includes introduction of block copolymers and maleated polymers as compatibilizers to assemble at polymer-polymer interface and improve the interfacial adhesion between the polymers.[4]

Many plastics require the use of reinforced materials, and the high surface area of nanoparticles has proven to be particularly effective in reinforcing polymers.[5] Some nanoparticles have been shown to settle at the interface between the polymers, modifying the interfacial energy while offering their own intrinsic functionalities in the blend. These particles have also been used for toughening polymers by enhancing the elastic properties of the polymer. Elias et al.[6] found out silica nanoparticles segregated both in the poly(ethylene-co-vinyl acetate) phase and in the

interface of polypropylene/poly(ethylene-co-vinyl acetate) (80/20), thereby acting as a compatibilizer between the polymers. Unfortunately, aggregation and agglomeration of nanoparticles prevent the nanocomposite from reaching its full potential due to the increased agglomerate size, which reduces effective surface area and creates point defects in the polymer[7–12] Agglomeration of nanoparticles in polymers reduces the nanoparticle/polymer interface area and leads to the formation of weaker spots in the form of voids due to the relatively weak cohesion between the aggregated nanoparticles and the matrix.[13] The final dispersion state of nanoparticles in a polymer matrix is critical in determining the properties of the nanocomposite. One factor is the radius of gyration (R_g) of the polymer chains and the nanoparticle. If the R_g of the polymer chain is greater than the R_g of the nanoparticle, the thermodynamic stability of the filled polymer is enhanced. On the contrary, if the R_g of nanoparticle is significantly greater than the R_g of the polymer chain, there is a mismatch in the surface energy between the polymer and the nanoparticle and this leads to aggregation of the nanoparticles.[14] Enthalpic interactions also affect the dispersion of these particles in the polymer matrix. If the surface of the particle is chemically similar to that of the polymer matrix, compatibility between the particle and the matrix is improved.[4] This enthalpic interaction favors the dispersion or aggregates and even distribution of the nanoparticle in the polymer matrix.[14]

Aramid nanofibers (ANFs) are aromatic polyamide nanofibers with high chemical, temperature and fatigue resistance, which makes them interesting for their potential to reinforce polymer matrices. [15–17] ANFs are prepared through the dissolution of macroscale polyamide fibers in dimethyl sulfoxide (DMSO) with controlled deprotonation using potassium hydroxide (KOH) at high concentrations. Following their production, ANFs possess a charged surface in the DMSO/KOH solution (shown in **Figure 1b**). ANFs have been used in making high strength

polymer nanocomposites due to their hydrogen bonds and pi-pi interactions easily formed with polymers that have chemical structure similarities with ANFs.[18,19] ANFs show poor compatibility with polymers of different chemical structure or those that do not promote hydrogen bonding. Several works have demonstrated that ANFs and their composites have potential use in many fields including high strength composites, adsorption, energy storage and filtration.[20–22] For example, Jung et al.[23] bonded modified cellulose nanocrystals to aramid nanofiber to form novel fillers for reinforcement of rubber compounds for tire applications. The reinforced rubber showed improvement in mechanical properties and crosslink density compared to non-reinforced rubber. Nasser et al.[24] also studied several aramid nanofibers filled thermoplastic nanocomposites prepared via solution casting. They found that the performance of the nanocomposite was dependent on the similarity of the matrix with the ANF's chemical structure. An increase of 62% and 27% was reported for the tensile strength of aramid nanofiber reinforced polyamide and polyamide-imide respectively, while ANF-filled polyimide did not show a significant increase in tensile strength. The difference in the performance of these nanocomposites was attributed to the ability of the ANF to form amide-amide hydrogen bonding in polyamide and polyamide-imide matrix but not in polyimide matrix.

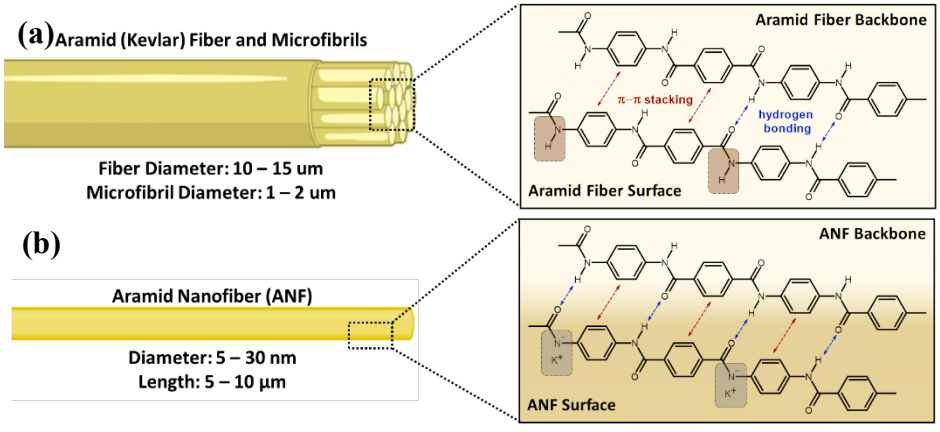

Figure 1. (a) Aramid fiber and microfibrils. (b) Deprotonated aramid nanofiber showing charged surface.

Modified ANFs have opened the door to improved dispersion of ANFs in reinforced/compatibilized plastics. Aramids typically phase separate in polymers; however, the addition of epoxy groups on the ANF backbone demonstrates that aramids with compatibilizing segments can improve dispersion and offers improved mechanical behavior in the single or mixed plastic systems. Jung et al.[25] showed improved dispersion and 16% and 14% increase in the modulus and strength, respectively, of an epoxy modified ANF in a simple epoxy system. Zhang et al.[26] showed improvements obtained with an epoxy modified ANF compatibilizer in a carboxylate acrylonitrile butadiene rubber (XNBR) and styrene butadiene rubber (SBR) blend. XNBR and SBR are immiscible and show inferior properties when mixed. The tensile and tear strength of the XNBR/SBR blends improved by as much as 87.2% and 194.7% through addition of only 0.3 wt. % of the epoxy modified ANF compatibilizer. Allyl and benzyl modified ANFs improved the mechanical properties of polystyrene composite films including toughness, Young's modulus and yield strength.[27]

Blending PP with PET offers some advantages such as PET enhancing the stiffness of PP at high temperatures while PP facilitating crystallization of PET by heterogeneous nucleation.[28]. Overall, PET has the tendency of improving the properties of PP, but the immiscibility of both polymers is a major drawback. [29,30] To the best of our knowledge, the effects of polymer grafted aramid nanofibers in immiscible blends have not been studied. The aim of this paper is to study the effects of aramid nanofiber and polymer grafted aramid nanofiber on the morphology, rheological and thermal properties of immiscible blends. A blend of waste PP and waste PET is used as a model immiscible polymer waste in this work.

2. Experimental Section/Methods

2.1. Materials

Waste polypropylene (PP) labware was obtained from the chemistry laboratory of the University of Massachusetts Lowell. The size of waste PP labware was reduced by a granulator (Model 1212, Cumberland engineering, New Berlin, WI, USA). Poly(ethylene terephthalate) (PET) from beverage bottles was obtained from UltrePET LLC (NY, USA), already washed and shredded into flakes. Aramid fiber (Kevlar, DuPont) pulp was obtained from Fiber Glast (Brookeville, OH). ANFs were prepared through the well-documented dissolution of the pulp fibers in dimethyl sulfoxide (DMSO) (Sigma Aldrich, USA) with controlled deprotonation using potassium hydroxide (KOH) (Sigma Aldrich, USA). 2.2 kilograms of DMSO and 3 wt. % each of KOH and aramid fiber pulp were mixed at 60 ˚C for 8-24 hours. The resultant solution was filtered and dried. It was observed that the resulting ANFs could not readily dispersed into any other solvent system outside of the original DMSO/KOH solution. The DMSO/KOH solvent system is therefore vital to production of the ANFs as well as any further modifications, as it created a reactive scaffold for additional surface chemistry modifications. Epoxy modified ANFs (epoxy-ANF) were prepared by re-dispersing ANFs into the DMSO/KOH suspension and diluting the mixture with additional DMSO to reduce viscosity. Excess epichlorohydrin (Sigma Aldrich, USA) was added dropwise to the solution under heavy stirring. The reaction vessel was sealed under nitrogen and allowed to react for 24 hours at 40 °C. Cold water was added to the final solution to precipitate the epoxy-ANFs before they were filtered and dried in a vacuum oven overnight at 90 °C.

One of two proprietary coupling agents (Luna Labs) was added to the epoxy groups on the epoxy-ANF to enable a grafting-to approach with either PET or PP. For a typical reaction, epoxy-ANFs were re-dispersed in the DMSO/KOH solution before diluting with DMSO to reduce the viscosity. The coupling agent was added, and the reaction mixture was heated to 75°C for 24 hours.

The resulting dark red suspension was then precipitated in toluene, filtered, and dried in a vacuum oven at 60 °C for 24 hours. Two distinct modified ANFs were prepared to graft either a functionalized PET (~4,000 g/mol) or functionalized PP (~10,000 g/mol) to the surface of the ANFs. For the PET grafting to approach, 10 g of ANFs with the appropriate coupling agent and 60 grams (excess) of the functionalized PET were dispersed in 950 mL of DMSO and heated to 140 ºC. The reaction was allowed to proceed for 72 hours before cooling. The resulting PET_ANF was precipitated in 2 L of water, filtered, and run under a Soxhlet extractor using chloroform to remove impurities. On average, the reaction resulted in the addition of 8 g of PET to every 1 g of ANF. For the PP grafting to approach, 3 g of ANFs with the appropriate coupling agent and 60 grams of the functionalized PP were dispersed in 900 mL of toluene and 100 mL of DMSO and heated to 150 ºC. The reaction was allowed to proceed for 72 hours before cooling. The resulting PP_ANF was precipitated in 2 L of water/isopropanol (70/30), filtered with water/isopropanol, and dried under vacuum at 60 °C for 24 hours. The resulting powder was washed with chloroform using a Soxhlet extractor over 24 hours and dried again at 60 °C for 24 hours. The reaction resulted in the addition of 20 g of PP to every 1 g of ANF. Purification of the PET_ANF and PP_ANF materials resulted in light brown to white powder that was a combination of the yellow Kevlar coated in a white PET or PP polymer. The ungrafted and grafted aramid nanofibers were provided by Luna labs. (VA, USA).

2.2. Blend preparation

Blends of PP/PET were prepared in several weight ratios (100/0, 10/90, 50/50, 90/10 and 0/100) with 0.5 g of the nanofiber and modified nanofiber in the blends. Samples were analyzed and a formulation of PP/PET at 90/10 weight ratio was selected for further processing analysis. This formulation was selected because a previous study showed that lower loading of contaminant

polymers such as PET in PP affect the mechanical properties of PP.[31] For the selected ratio (i.e., PP/PET at 90/10), several blends were prepared by adding 0, 1, 2 and 5 weight percent of aramid nanofiber (ANF), PET-modified aramid nanofiber (PET_ANF) and PP-modified aramid nanofiber (PP_ANF). Prior to compounding of the blends, PET and PP materials were dried at 110 °C for 4 hours in an oven (Model FD 56, Binder GmbH, Tuttlingen, Germany).[32]

The blends were prepared using a conical twin screw micro compounder (Xplore^{TM} HT-15, Sittard, The Netherlands) at 280 °C and 50 rpm to achieve good melting of both PET and PP and allow dispersion of the aramid nanofibers.

2.3. Characterization of blends

2.3.1. Dispersion of Functionalized Aramid Nanofiber in Solvents

Aramid nanofiber (ANF), PET-grafted aramid nanofiber (PET_ANF), and PP-grafted nanofiber (PP_ANF) were dispersed in water, xylene (Sigma Aldrich, USA) and chlorophenol (Sigma Aldrich, USA) at a concentration of 0.25 mg/ml to determine the dispersion of the nanofibers in the solvents. All nanofibers dispersed in xylene were heated at about 60°C for 10 minutes to explore the suspension behavior at elevated temperature.

2.3.2. Scanning Electron Microscopy

A scanning electron microscope (SEM, JEOL JSM 6390, Tokyo, Japan) was used to investigate the morphology of the blends. Prior to the microscopy, samples were fractured in liquid nitrogen and coated with gold for 120 seconds using a vacuum sputter coater (Denton vacuum desk IV, Denton Vacuum, LLC, Moorestown, NJ, USA). The images were taken at an accelerating voltage of 15kV [33] and a magnification of 1000x. The droplet size distribution in the PP matrix was quantified by using Image J (version1.53k).

2.3.3. Rheology

Rheological analysis of samples was performed using an ARES-G2 rotational rheometer (ARES-G2, TA Instruments, New Castle, DE, USA). Disks with a 25 mm diameter and thickness of 1.6 mm of pre-dried flakes and pre-dried blends were molded using a micro injection molding machine (Xplore^{TM} Instruments BV, Sittard, The Netherlands) at 280 °C. A parallel plate geometry of diameter 25 mm set a constant gap size of 1.6 mm was used. Strain sweeps were carried out at 260 °C to define the linear viscoelastic region (LVR) and select a strain percentage for the frequency sweep test (shown in **Figure S1)**. A strain percentage of 5% was selected for the frequency sweep over an angular sweep of 0.0628 to 628 rad/s.

2.3.4. Differential Scanning Calorimetry

A differential scanning calorimeter (Mettler Toledo LLC, Columbus, OH, USA) was used to determine the effects of aramid nanofibers on the thermal properties of the blend. Samples (3-7 mg) were heated at 10 °C /min to 300 °C and allowed to melt isothermally at 300 °C for 5 minutes. The samples were cooled at 10 °C/min to -50 °C and the heating protocol was repeated. The second heating was used to analyze the change in enthalpy of fusion.

2.3.5. Tensile test

Tensile tests were performed on a tensile testing machine (Instron® 5966, Norwood, MA, USA) to determine the mechanical properties of the blends according to ASTM D638 using the tensile. Prior to testing, samples were molded into Type IV tensile bars using micro injection molding machine (Xplore^{TM} Instruments BV, Sittard, The Netherlands) at 280 °C. Samples containing 5% of the aramid nanofiber were tested because these samples showed better interactions with the polymers. Due to insufficient amount of samples, only three specimens of

unfilled blends and 5% ANF, whereas five specimen were tested for 5% PET_ANF and 5% PP_ANF.

3. Results and Analysis

3.1. Dispersion of aramid nanofiber in solvents

The aim of this experiment was to qualitatively assess the compatibility of the polymer grafted aramid nanofiber with its constituent polymer when blended. Nanoparticles grafted with

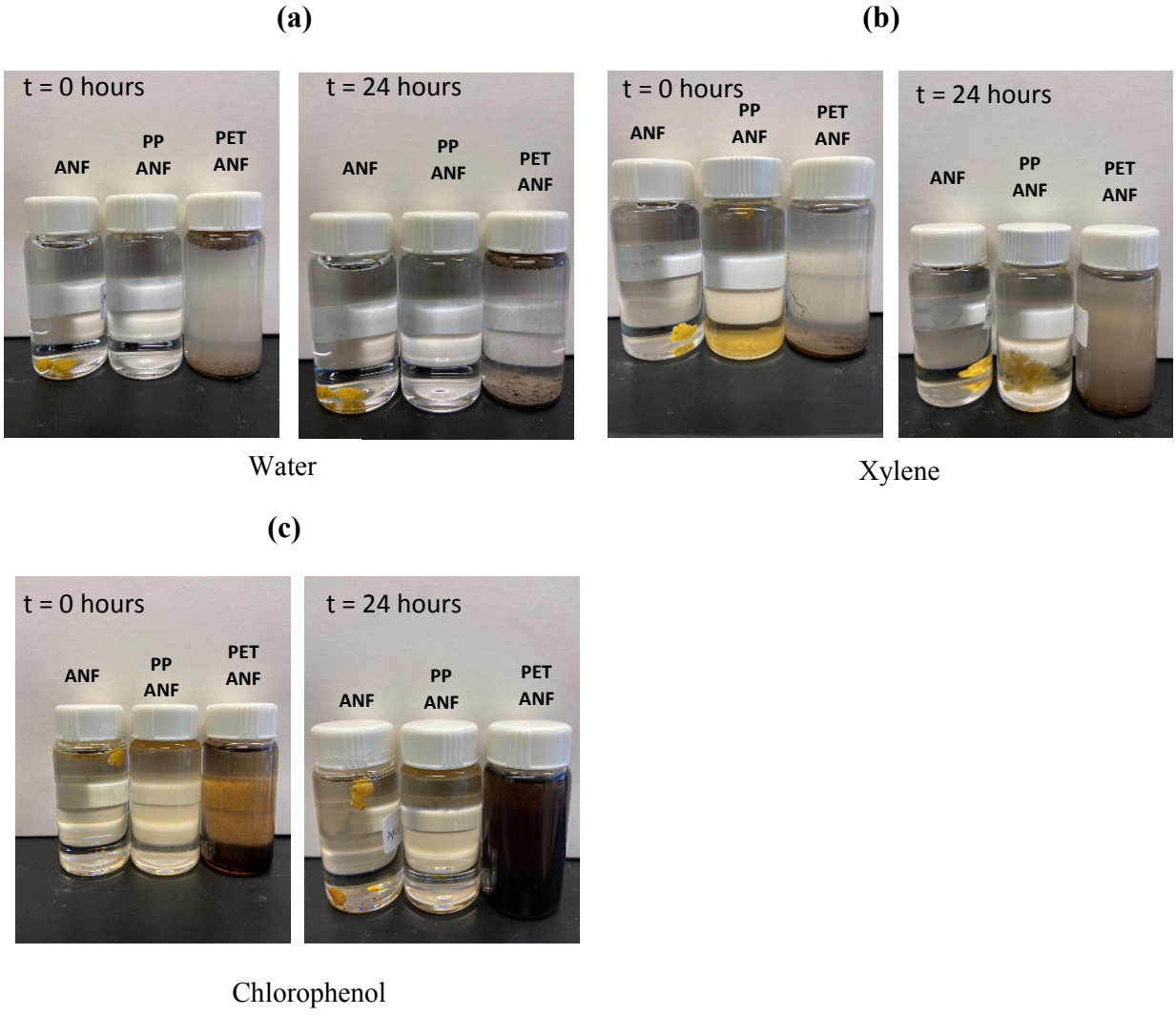

Figure 2. Suspension of unmodified aramid nanofiber and polymer grafted aramid nanofiber in (a) water, (b) xylene and (c) chlorophenol at t=0 and t=24 hours (note: Fig 1b shows PP in xylene at a temperature of about 60 °C).

polymer chains have been found to have better dispersion in a matrix of that polymer. Thus, successful suspension in a good solvent for the grafted polymer should confirm the modification to the surface energy.[34] As shown in **Figure 2a**, ANF and PET_ANF settled at the bottom of the vial when dispersed in water; however, PP_ANF floated on the surface of water due to the hydrophobicity and lower density of the PP component of PP_ANF.[35] After 24 hours, there was no significant change in the water containing ANF, PP_ANF and PET_ANF.

ANF samples dispersed in xylene (**Figure 2b**) settled at the bottom of the vial whereas PET_ANF was cloudy at t = 0 but became clearer with a visible separation between PET_ANF and the solvent. This shows the incompatibility of polar PET_ANF with xylene. Both ANF and PET_ANF dispersed in xylene showed significant changes after 24 hours. PP_ANF dispersed in xylene at time t = 0, settled at the bottom of the vial. After 24 hours, PP_ANF appeared to swell in xylene after heat was applied for 5 minutes at a temperature of about 60 °C, which provides further evidence of the surface modification since PP is soluble in high temperature xylene.[36] The swelling of PP_ANF could be correlated to the solvent uptake of the PP portion of the PP_ANF. ANF and PET_ANF samples suspended in xylene remained the same. Typically, polyolefins have a good solubility in xylene because they share similar polarity and dispersion forces. This indicates that when PP_ANF is added to PP/PET blend, PP_ANF will show greater affinity towards PP matrix of the PP/PET blend.[36]

Shown in **Figure 2c**, when samples were suspended in chlorophenol, there was no change in the ANF suspension after 24 hours. There was also no color change or cloudiness in the PP_ANF-chlorophenol suspension after 24 hours. There was a visible separation between PP_ANF and chlorophenol where PP_ANF floated at the top due to its lower density and surface tension effects. Some PET_ANF was visible at the bottom of the vial; however, the colorless

chlorophenol solvent became dark yellow indicating some dispersion of the PET-grafted ANF in the solvent. The color of PET_ANF in PET_ANF-chlorophenol intensified after 24 hours. The mixture was dark yellow and became intense dark yellow after 24 hours. This shows the affinity of PET_ANF for chlorophenol since both are polar and PET has some solubility in chlorophenol.[36] In general, these results indicate that the surface of the nanofibers was successfully modified after the grafting reactions.

3.2. Morphology

SEM was carried out to evaluate the morphology of PP/PET 90/10 blends. Images of fractured surfaces of blends are shown in **Figure 3**. The blend without any filler shows droplets in the PP matrix. This may be ascribed as the dispersed PET in the PP matrix. No ANF particles were visible in the SEM images; however, an analysis of the PET droplet size was undertaken to understand the effects of the various functionalized ANF on the blend morphology. The PET dispersed phase in the matrices of blends containing 1% and 2% nanofibers is roughly spherical. At 5% loading level of PP_ANF, the PET droplet phase was not visible. The size of about 100 droplets of the dispersed phase for samples containing 1% and 2% of the nanofiber was determined using Image J. Fewer than 100 droplets were analyzed for samples containing 2% and 5% PP_ANF due to the lower numbers of droplets observed, which is caused by the shape irregularity of the dispersed phase. A violin plot (**Figure 4**) shows the droplet size distribution of the various samples. **Figure 4a** shows the droplet distribution of unfilled PP/PET blend while **Figure 4b**, **4c** and **4d** shows the droplets size distribution of filled samples at 1%, 2% and 5% loading levels respectively. Generally, PP_ANF filled samples showed a decrease in the droplets size and a more uniform morphology irrespective of the loading level. At 1% and 2% loading level, it is seen that the average size of droplets in blends containing PP_ANF ranged between 0.5 to about 2 μm, while

samples with ANF and PET_ ANF showed larger droplet sizes. At 5% loading level of PP_ANF (**Figure 4d**), there was difficulty in discerning the number of droplets in the images. Hence, only 8 droplets were observed, and this may not be a true representation of the number of droplets in the blend. This could be caused by a significant decrease of the droplet size, making them difficult to observe under SEM. This may be attributed to the compatibility of PP and PET with 5% PP_ANF.[37] For 5% loading level of PET_ANF, there was an increase in coalescence of the droplets, forming large domains of the dispersed phase and irregularity in the shapes of the droplets. Thus, it is difficult to discern droplets in the image and only a few droplets were analyzed. In conclusion, polymer grafted nanofiber showed affinity for its like polymers.

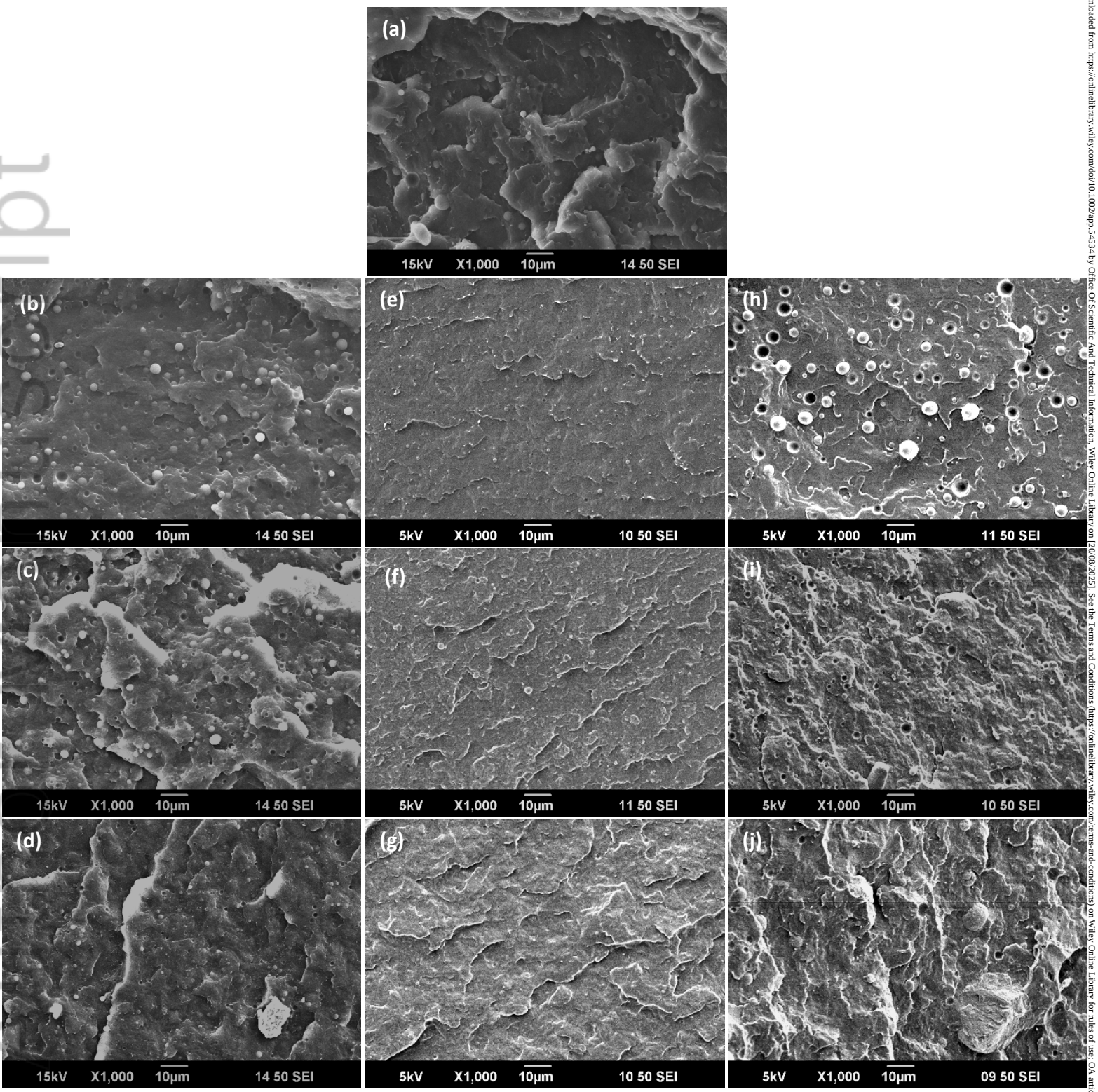

Figure 3. SEM images of PP/PET 90/10 blends. (a)PP/PET (b) ANF1% (c) ANF2% (d) ANF5% (e) PP_ANF1% (f) PP_ANF2% (g) PP_ANF5% (h) PET_ANF1% (i) PET_ANF2% (j) PET_ANF5%

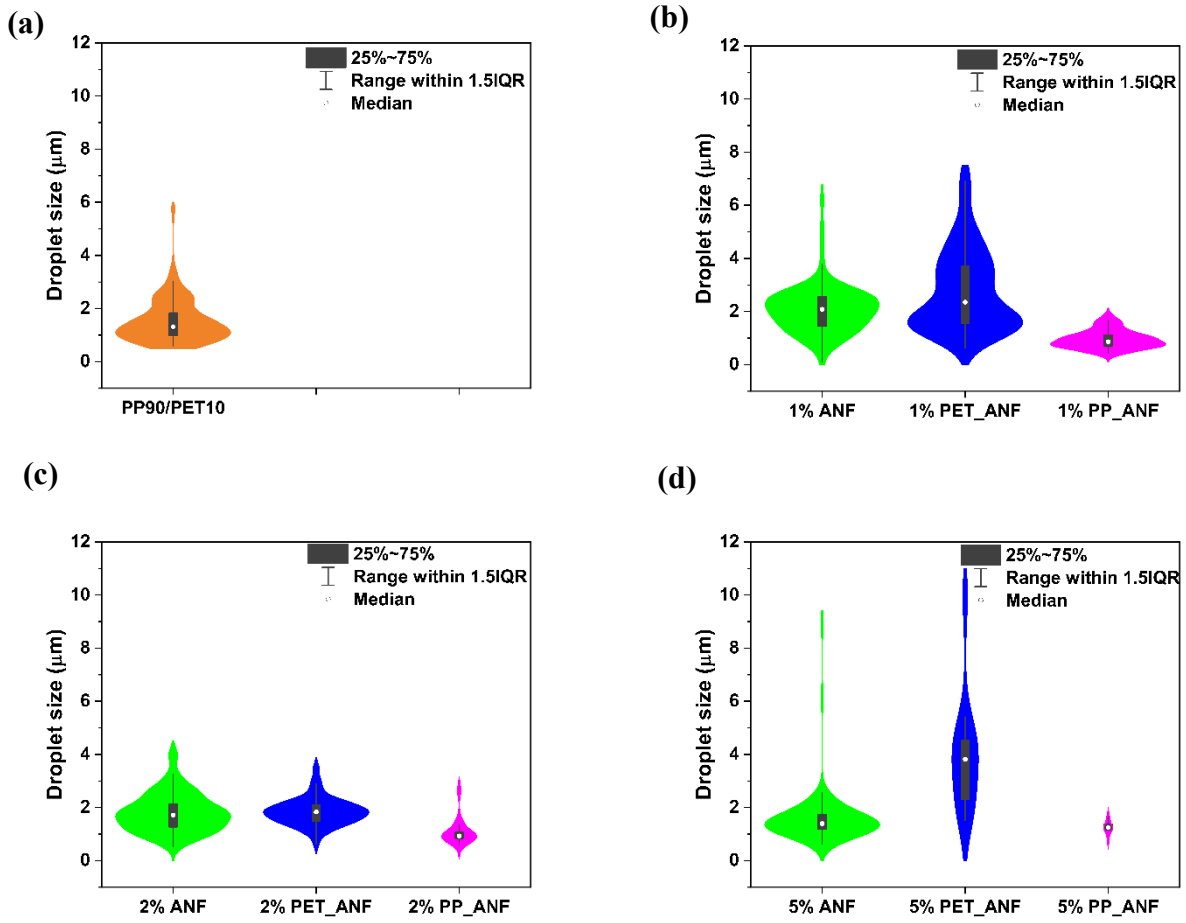

Figure 4. Violin plot showing the droplet size distribution for (a) PP/PET (b) 1% (c) 2% (d) 3% filled samples.

3.3. Rheology

Melt rheology can reveal features of the mechanical response of polymer blends and composites related to the molecular weight of constituent polymers, phase morphology in immiscible blends, and the degree of dispersion and interfacial affinity between solid fillers and molten polymers. **Figure 5**. Shows the complex viscosity of all the blends. **Figure 5a** shows the viscosity of waste PET, PP, and unfilled PP/PET blend. The viscosity of the PET waste is much lower compared to waste PP and PP/PET blend, and it is Newtonian over the whole frequency

range investigated. Addition of 10% PET to PP slightly lowers its overall viscosity. An upturn in the complex viscosity is evident at lower frequency for waste PP and waste PP/PET blend. The viscosity decreases over all frequencies for samples containing unmodified ANF and PET_ANF with an increase in the loading level. This contradicts the Einstein equation, which predicts the change in viscosity of a liquid suspension of solid particles. The Einstein equation gives viscosity as $\mu(1+2.5\varphi)$, where μ is the original liquid viscosity and φ is the volume fraction of the filler, predicting an increase in the viscosity of the matrix with an increase in the volume fraction of the filler.[38] This shows that this expression does not hold for blends with ANF and PET_ANF. Earlier studies have attributed a decrease in viscosity to polymer degradation, excluded free volume around the nanoparticles,[39] a slip between the polymer chains and the nanoparticles,[40] or selective adsorption of high molecular weight polymer chains on the surface of the nanoparticle.[41] Prior literatures also showed a similar decrease in the viscosity of the nanoparticle filled polystyrene with the addition of PS nanoparticles chosen for the neutral chemical interaction with the polystyrene polymer matrix in a study to investigate the unusual decrease in filled linear polymers.[38 42]. This decrease in viscosity of the filled polystyrene was attributed to the excluded free volume induced around the nanoparticle. In another study,[40], the decrease in viscosity with an increase in silica content in a silica filled poly(ethylene 2,6 – naphthalate) nanocomposite was observed. It was found that the spherical and smooth non-porous shape of the nanoparticle lowered the friction coefficients in the silica filled poly(ethylene 2,6 – naphthalate). Thus, the nanoparticle acted as a lubricant during compounding. **Figure 5c** shows a slight increase in viscosity at lower frequency for PP_ANF samples, as well as an overall retention of similar viscosity to the unfilled blend. This may be due to the PP-PP_ANF interactions which restricts the mobility of the polymer chains at the interface.[43]

Storage moduli and loss moduli of blends as a function of aramid nanofiber content are presented in **Figure 6** and **Figure S5** respectively. **Figure 6a** shows that all samples containing ANF have a plateau in G' at lower frequencies, and this corresponds to the presence of a dispersed phase of particles that are able to form a network.[44,45] This plateau is prominent at 5% weight loading level.

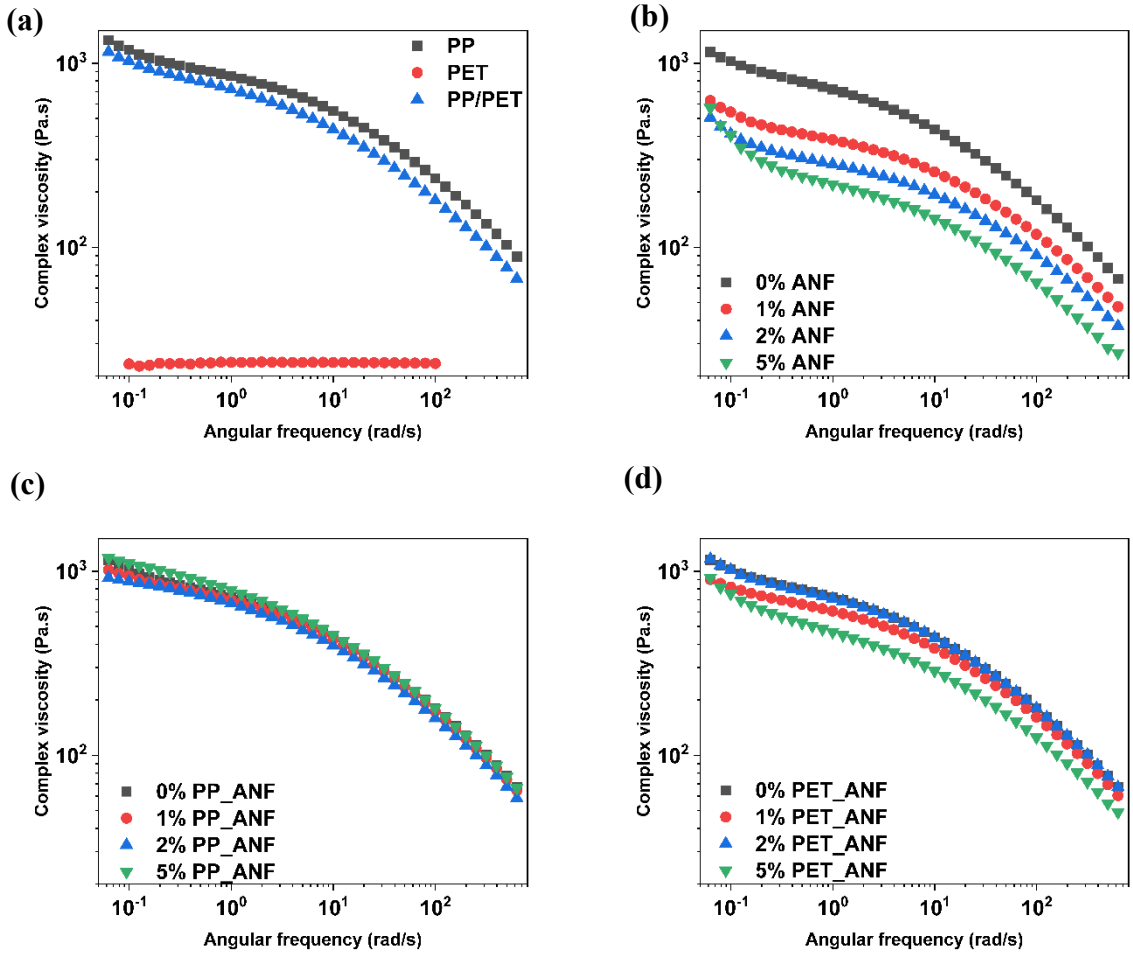

Figure 5. Complex viscosity results for (a)PP, PET, and unfilled PP/PET (b) PP/PET/ANF, (c) PP/PET/PP_ ANF and (d) PP/PET/PET_ANF samples.

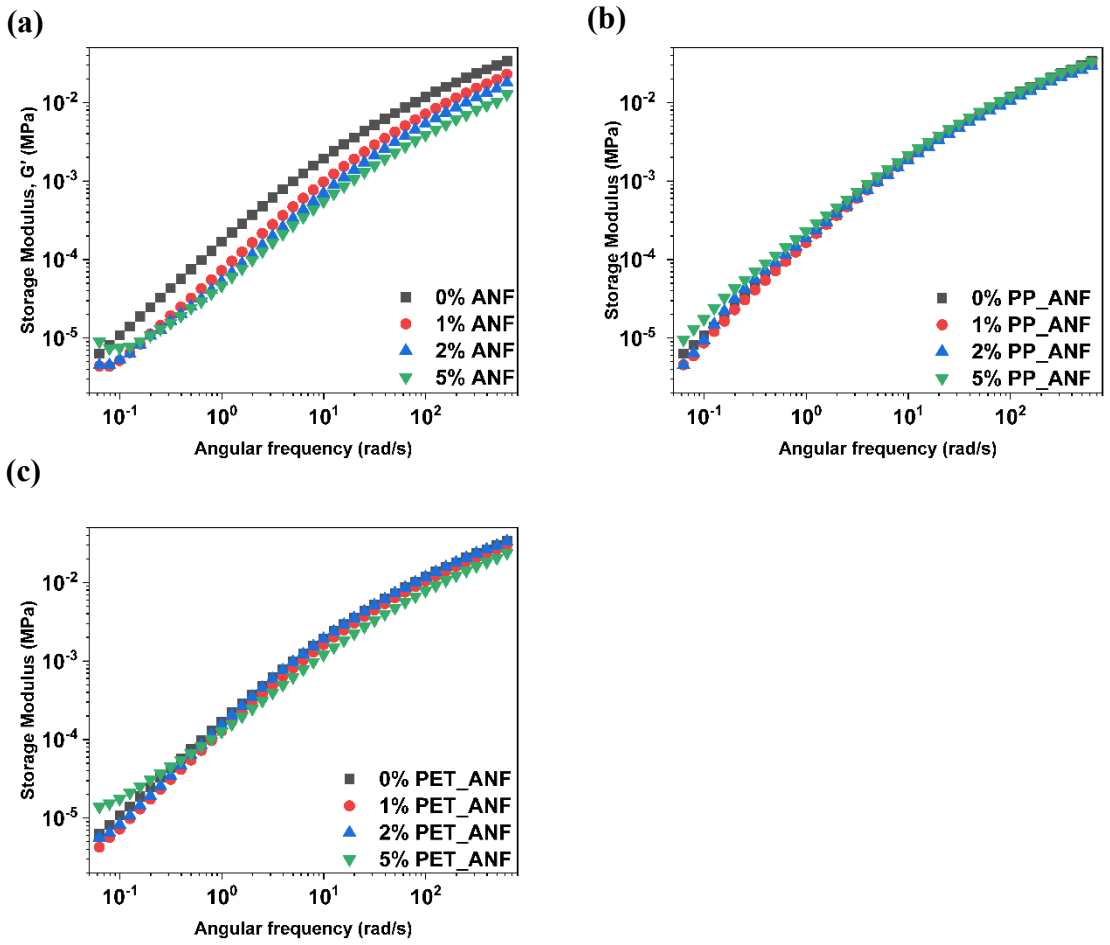

Figure 6. Storage modulus of (a) PP/PET/ANF, (b) PP/PET/ PP ANF and (c) PP/PET/PET ANF at different loading levels at 260°C

From **Figure 6c** the plateau is seen clearly at the highest loading level of PET_ANF. The plateau of the storage modulus at lower frequency may be caused by the restriction at the interface of the blend, droplet recoil and the presence of the aramid nanofiber in one of the phases.[44] This plateau-like behavior is reported in other studies, and it suggests the structure of the blend can support stress either through networking of the particles or elasticity at the droplet interfaces. [46–49] The alteration of storage modulus at lower frequency can be used to determine the polymer-filler interfacial interactions, particle dispersion and agglomeration issues and formation of physical network in the polymer.[50] For PP_ANF filled samples in **Figure 6b**, no solid-like plateau is observed at lower frequency because PP_ANF did not form a network in the major phase (i.e.,

PP), which controls the bulk rheology.[51] We speculate that the 5% loading still leaves room for the individual PP_ANF particles to remain separate in the PP phase, whereas in the case of PET_ANF, the 10% PET droplets take up a large fraction of the filler and a network can form. However, the slight increase in storage modulus of PP at low frequency could be explained by an increased interaction between PP and PP_ANF which leads to some restriction of the long-range mobility of the chains in the matrix.[52] This suggests the affinity of PP grafted aramid nanofiber towards the PP component of the blend. In summary, unmodified aramid nanofiber has the tendency to reduce the viscosity and elasticity of the blend due to its immiscibility with PP and PET, whereas PP grafted aramid nanofiber filled blend showed similar viscoelastic behavior as the unfilled blend. Incorporating 5% PP_ANF in the PP/PET blend presents a better interaction between the droplets and the matrix compared to 1% and 2% PP_ANF. This supports the morphology results in which only a few droplets are seen at 5% loading level of PP_ANF.

3.4. Differential Scanning Calorimetry

Understanding the effects of aramid nanofiber on the crystallinity and nucleation in each polymer is necessary for determining the relationships between processing and mechanical properties in the blends. **Figure S2, S3** and **S4** show the first cycle melting endotherms, crystallization exotherms and second cycle endotherms of the blends, respectively. **Figure 7a** and **7b** illustrate the crystallization exotherms and melting endotherms of the blends with 5% nanofiber, respectively.

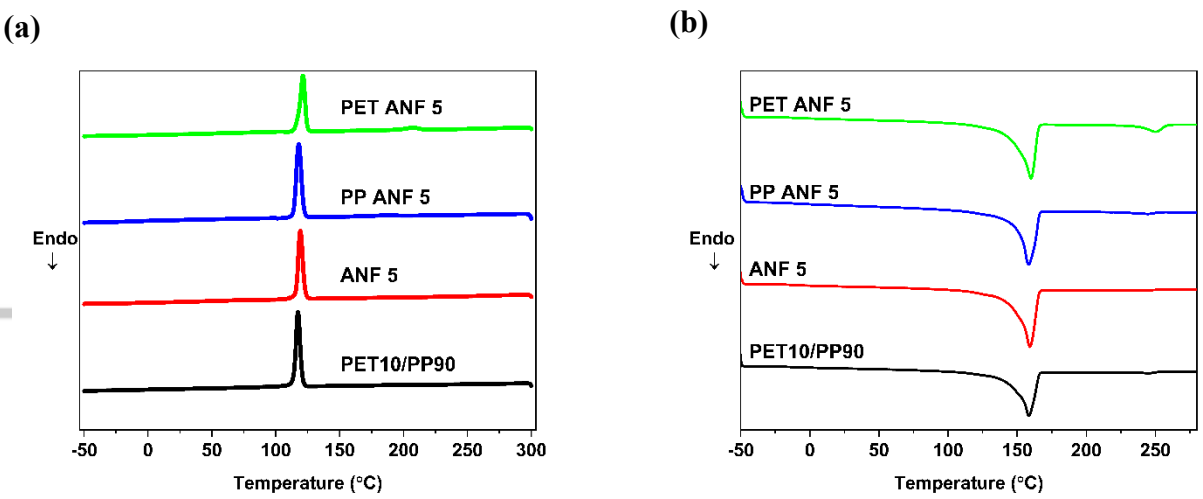

Figure 7. (a) Crystallization exotherms and (b) melting endotherms of blends with 5% loading level of aramid nanofibers

The crystallization peak of PET (around 200°C) is only visible for samples containing PET_ANF. This indicates that the addition of PET_ANF facilitated nucleation of PET. The melting temperature and enthalpies are given in **Tables 3** and **4**. The melting temperature of PET did not change significantly, nor did the enthalpy of fusion of the PET portion of the blends containing ANF and PP_ANF. In contrast, both the melting temperature and the enthalpy of fusion of PET portion of the blends increased with increasing level of PET_ANF loading. This indicates that PET_ANF have preferential interaction and affinity towards the PET dispersed phase.[53] There were no significant changes in melting temperatures of the PP portion of the blend; however, the enthalpy of fusion of samples containing ANF and PP_ANF decreased when compared with the unfilled PP/PET blend. This may be ascribed to an interference of the nanoparticles in the crystallization process of PP.[54] The enthalpy of fusion of the PET portion of the blend increased for the samples with higher PET_ANF; this may indicate again some ability of the PET_ANF to act as a nucleating agent.[55] This confirms polymer grafted aramid nanofiber interacts with its like polymer.

Table 3. Thermal properties of PET fraction of blend obtained from the first endotherm.

	ANF		PET_ANF		PP_ANF	
Wt%	Tm (°C)	ΔH_f (J/g)	Tm (°C)	ΔH_f (J/g)	Tm (°C)	ΔH_f (J/g)
1	241.5 ± 3.6	3.0 ± 0.1	246.5 ± 0.5	3.1 ± 0.3	244.7 ± 0.9	2.3 ± 0.3
2	245.6 ± 1.0	3.3 ± 0.5	247.6 ± 0.9	3.7 ± 0.6	244.2 ± 1.2	2.2 ± 0.5
5	245.2 ± 1.1	3.1 ± 0.9	249.8 ± 0.4	5.6 ± 1.3	245.1 ± 1.82	2.5 ± 2.0

Note: T_m and H_f of PET fraction in neat PP/PET blend are 245.2 °C and 1.69 J/g respectively.

Table 4. Thermal properties of PP fraction of blend obtained from the second heating.

	ANF		PET_ANF		PP_ANF	
Wt%	Tm (°C)	ΔH_f (J/g)	Tm (°C)	ΔH_f (J/g)	Tm (°C)	ΔH_f (J/g)
1	158.0 ± 0.5	87.6 ± 1.7	158.1 ± 2.1	87.0 ± 6.7	157.1 ± 1.0	84.6 ± 2.8
2	157.8 ± 0.5	84.6 ± 1.0	159.3 ± 0.5	87.5 ± 4.8	159.6 ± 2.0	83.9 ± 2.1
5	156.4 ± 0.4	86.8 ± 5.0	158.1 ± 0.4	85.3 ± 4.4	157.1 ± 1.1	84.5 ± 2.6

Note: T_m and H_f of PP fraction in neat PP/PET blend are 158.5 °C and 90.69 J/g respectively.

3.5. Tensile test

The tensile modulus and elongation at break of the blends were compared. Figure 8 (a) and (b) show the tensile modulus and elongation at break of the blends respectively. When compared with the unfilled PP/PET blend, the tensile modulus of the filled blends increases irrespective of the type of aramid nanofiber. PP_ANF filled samples showed the highest tensile modulus followed by PET_ANF filled samples. This confirms the reinforcement effects of the polymer modified aramid nanofibers. However, the elongation at break of the filled samples was lower than unfilled PP/PET blend except for the PP_ANF filled blend which showed a comparable elongation at break.

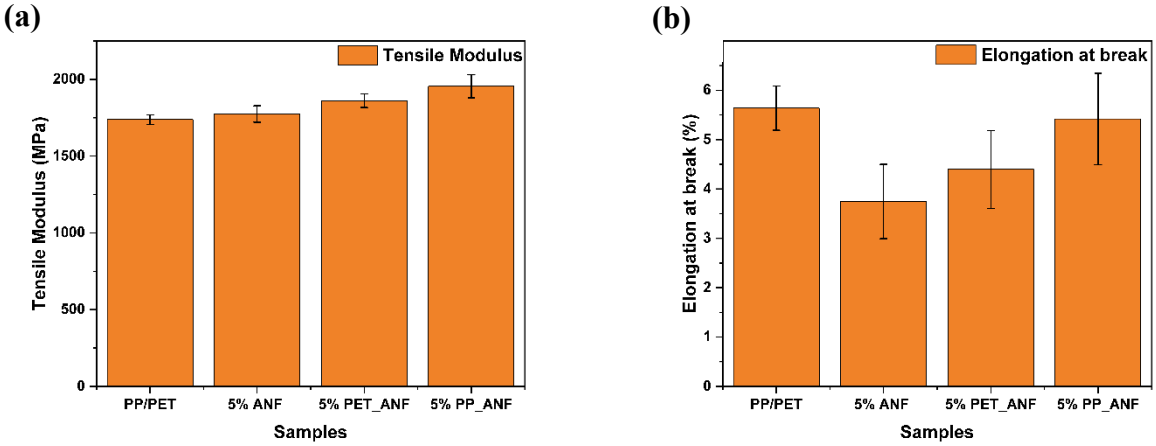

Figure 8. (a) Tensile modulus and (b) elongation at break of samples filled with 5% of different types of aramid nanofiber

4. Conclusion

In summary, this study has shown the affinity of polymer grafted aramid nanofiber towards its like polymer in an immiscible blend. We showed that PP_ANF enhanced the rheological properties of the blend since PP is the matrix and controls the bulk rheology. This confirms the miscibility of PP grafted aramid nanofiber to PP as compared to unmodified aramid nanofiber. We also confirmed the affinity of polar PET_ANF and nonpolar PP_ANF to polar chlorophenol and nonpolar xylene, respectively, by suspending the aramid nanofibers in solvents. SEM showed good dispersion of PET droplets in the PP matrix of the immiscible blend when PP_ANF is added. This shows that grafting PP to ANF could enhance its dispersion in PP nanocomposite and reinforce the nanocomposite. Agglomeration of nanofibers in nanocomposites could be reduced by grafting like-polymers onto the aramid nanofibers. Incorporating neat ANF and PET_ANF in a PP blend reduces the viscosity of the blend, potentially due to an increase in free volume, or to polymer degradation. Grafting aramid nanofibers with polymers can improve the compatibility of these

nanofibers with polymers while reinforcing the polymers in the blends. In future, aramid nanofiber can be grafted with both PET and PP to enhance its affinity for both polymers in the blend. This could serve as an effective compatibilization scheme while also providing reinforcement to the polymer blend. This study highlights blending and reinforcement as strategies to improve mechanical recycling of immiscible plastic waste.

Supporting Information: Additional supporting information can be found online in the Supporting information section at the end of this article.

Author Contributions: Conceptualization, S.M., A.T., J.K., M.S. and W-T.C.; methodology, S.M., A.T., J.K., M.S. and W-T.C; software, S.M. ; validation, S.M. and A.T. ; formal analysis, S.M. ; investigation, S.M., A.T., J.K., M.S. and W-T.C.; resources, J.K., M.S., W.-T.C.; data curation, S.M.; writing—original draft preparation, S.M.; writing—review and editing, S.M., J.K., M.S., and W-T.C.; visualization, S.M.; supervision, J.K., M.S., and W.-T.C.; project administration, J.K. and W.-T.C.; funding acquisition, J.K., M.S., and W.-T.C. All authors have read and agreed to the published version of the manuscript.

Funding: This material is based upon work supported by the U.S. Department of Energy's Office of Energy Efficiency and Renewable Energy (EERE) under the Bioenergy Technology Office (BETO) and the Advanced Manufacturing Office (AMO) Joint Topic (Award Number DE-SC0021790). This report was prepared as an account of work sponsored by an agency of the United States Government. Neither the United States Government nor any agency thereof, nor any of their employees, makes any warranty, express or implied, or assumes any legal liability or responsibility for the accuracy, completeness, or usefulness of any information, apparatus, product, or process disclosed, or represents that its use would not infringe privately owned rights. Reference herein to any specific commercial product, process, or service by trade name, trademark, manufacturer, or

otherwise does not necessarily constitute or imply its endorsement, recommendation, or favoring by the United States Government or any agency thereof. The views and opinions of authors expressed herein do not necessarily state or reflect those of the United States Government or any agency thereof. The authors also would like to thank the University of Massachusetts Lowell for providing start-up funds.

Acknowledgments: The authors are grateful to Dr. Earl Ada for assisting with SEM characterization and Mr. Pat Casey for helping with DSC and Kevin Hartman of University of Massachusetts, Lowell Chemistry lab for the donation of their labware PP waste.

Conflicts of Interest: The authors declare no conflict of interest.

References

1. Anuar Sharuddin, S. D.; Abnisa, F.; Wan Daud, W. M. A.; Aroua, M. K. A review on pyrolysis of plastic wastes. *Energy Convers. Manag.* **2016**, *115*.

2. Ragaert, K.; Delva, L.; Van Geem, K. Mechanical and chemical recycling of solid plastic waste. *Waste Manag.* **2017**, *69*, 24–58.

3. Utracki, L. A.; Wilkie, C. A. *Polymer blends handbook*; **2014**.

4. Utracki, L. A. Compatibilization of polymer blends. *Can. J. Chem. Eng.* **2002**, *80*, 1008–1016.

5. Karak, N. In *Nanomaterials and Polymer Nanocomposites: Raw Materials to Applications*; **2018**.

6. Elias, L.; Fenouillot, F.; Majesté, J. C.; Alcouffe, P.; Cassagnau, P. *Polymer (Guildf).*

2008, *49*.

7. Kumar, S. K.; Jouault, N.; Benicewicz, B.; Neely, T. Nanocomposites with polymer grafted nanoparticles. *Macromolecules* **2013**, *46*.

8. Srivastava, S.; Agarwal, P.; Archer, L. A. *Langmuir* **2012**, *28*.

9. Chen, S. H.; Souna, A. J.; Stranick, S. J.; Jhalaria, M.; Kumar, S. K.; Soles, C. L.; Chan, E. P. *Soft Matter* **2022**, *18*.

10. Moll, J. F.; Akcora, P.; Rungta, A.; Gong, S.; Colby, R. H.; Benicewicz, B. C.; Kumar, S. K. *Macromolecules* **2011**, *44*.

11. Munaò, G.; De Nicola, A.; Müller-Plathe, F.; Kawakatsu, T.; Kalogirou, A.; Milano, G. *Macromolecules* **2019**, *52*.

12. Bahrami, R.; Löbling, T. I.; Schmalz, H.; Müller, A. H. E.; Altstädt, V. *Polymer (Guildf).* **2017**, *109*.

13. Endres, S. C.; Ciacchi, L. C.; Mädler, L. *J. Aerosol Sci.* **2021**, *153*.

14. Mackay, M. E.; Tuteja, A.; Duxbury, P. M.; Hawker, C. J.; Van Horn, B.; Guan, Z.; Chen, G.; Krishnan, R. S. *Science (80-.).* **2006**, *311*.

15. García, J. M.; García, F. C.; Serna, F.; de la Peña, J. L. High-performance aromatic polyamides. *Prog. Polym. Sci.* **2010**, *35*.

16. Cao, K.; Siepermann, C. P.; Yang, M.; Waas, A. M.; Kotov, N. A.; Thouless, M. D.; Arruda, E. M. *Adv. Funct. Mater.* **2013**, *23*.

17. Yang, M.; Cao, K.; Sui, L.; Qi, Y.; Zhu, J.; Waas, A.; Arruda, E. M.; Kieffer, J.; Thouless,

M. D.; Kotov, N. A. **2011**.

18. Kuang, Q.; Zhang, D.; Yu, J. C.; Chang, Y. W.; Yue, M.; Hou, Y.; Yang, M. *J. Phys. Chem. C* **2015**, *119*.

19. Lin, J.; Bang, S. H.; Malakooti, M. H.; Sodano, H. A. *ACS Appl. Mater. Interfaces* **2017**, *9*.

20. Zhang, B.; Wang, W.; Tian, M.; Ning, N.; Zhang, L. Preparation of aramid nanofiber and its application in polymer reinforcement: A review. *Eur. Polym. J.* **2020**, *139*.

21. Yang, B.; Wang, L.; Zhang, M.; Li, W.; Zhou, Q.; Zhong, L. Advanced separators based on aramid nanofiber (ANF) membranes for lithium-ion batteries: a review of recent progress. *J. Mater. Chem. A* **2021**, *9*.

22. Zhao, Y.; Li, X.; Shen, J.; Gao, C.; Van Der Bruggen, B. The potential of Kevlar aramid nanofiber composite membranes. *J. Mater. Chem. A* **2020**, *8*.

23. Jung, J.; Sodano, H. A. *Cellulose* **2022**, *29*, 7735.

24. Nasser, J.; Zhang, L.; Lin, J.; Sodano, H. *ACS Appl. Polym. Mater.* **2020**, *2*.

25. Jung, J.; Sodano, H. A. *Polymer (Guildf).* **2020**, *195*.

26. Zhang, X.; Chen, Y.; Yin, Q.; Wu, J.; Song, W.; Mohamed, A.; Jia, H.; Yang, F.; Rui, X. *Mater. Chem. Phys.* **2019**, *238*.

27. Peng, G.; Yaoqin, W.; Congcong, D.; Changmei, S.; Rongjun, Q.; Chunnuan, J.; Ying, Z.; Ying, W. *Front. Chem.* **2020**, *8*.

28. Papadopoulou, C. P.; Kalfoglou, N. K. *Polymer (Guildf).* **2000**, *41*.

29. Van Kets, K.; Jacques, J.; Delva, L.; Ragaert, K. *J. Appl. Polym. Sci.* **2021**, *138*.

30. Ahmadlouydarab, M.; Chamkouri, M.; Chamkouri, H. *Polym. Bull.* **2020**, *77*.

31. Luijsterburg, B. J.; Jobse, P. S.; Spoelstra, A. B.; Goossens, J. G. P. *Waste Manag.* **2016**, *54*.

32. Spasojević, P. M.; Panić, V. V.; Džunuzović, J. V.; Marinković, A. D.; Woortman, A. J. J.; Loos, K.; Popović, I. G. *RSC Adv.* **2015**, *5*.

33. Louwsma, J.; Carvalho, A.; Lutz, J. F.; Joly, S.; Chan-Seng, D. *Polymer (Guildf).* **2021**, *217*.

34. Sobkowicz, M. J.; Dorgan, J. R.; Gneshin, K. W.; Herring, A. M.; McKinnon, J. T. *Carbon N. Y.* **2009**, *47*.

35. Huang, Y.; Gancheva, T.; Favis, B. D.; Abidli, A.; Wang, J.; Park, C. B. *ACS Appl. Mater. Interfaces* **2021**, *13*.

36. Hansen, C. M. *Hansen solubility parameters: A user's handbook: Second edition*; **2007**.

37. Chen, D.; Tiwari, S. K.; Ma, Z.; Wen, J.; Liu, S.; Li, J.; Wei, F.; Thummavichai, K.; Yang, Z.; Zhu, Y.; Wang, N. *Polymers (Basel).* **2020**, *12*.

38. Mackay, M. E.; Dao, T. T.; Tuteja, A.; Ho, D. L.; Van Horn, B.; Kim, H. C.; Hawker, C. J. *Nat. Mater.* **2003**, *2*.

39. Tuteja, A.; Mackay, M. E.; Hawker, C. J.; Van Horn, B. *Macromolecules* **2005**, *38*.

40. Kim, S. H.; Ahn, S. H.; Hirai, T. *Polymer (Guildf).* **2003**, *44*.

41. Jain, S.; Goossens, J. G. P.; Peters, G. W. M.; Van Duin, M.; Lemstra, P. J. *Soft Matter*

2008, *4*.

42. Merkel, T. C.; Freeman, B. D.; Spontak, R. J.; He, Z.; Pinnau, I.; Meakin, P.; Hill, A. J. *Science (80-.).* **2002**, *296*.

43. Huang, H. X.; Zhang, J. J. *J. Appl. Polym. Sci.* **2009**, *111*.

44. Graebling, D.; Muller, R.; Palierne, J. F. *Macromolecules* **1993**, *26*.

45. Genoyer, J.; Yee, M.; Soulestin, J.; Demarquette, N. *J. Rheol. (N. Y. N. Y).* **2017**, *61*.

46. Sobkowicz, M. J.; White, E. A.; Dorgan, J. R. *J. Appl. Polym. Sci.* **2011**, *122*.

47. Mohammadi, M.; Heuzey, M. C.; Carreau, P. J.; Taguet, A. *Polymer (Guildf).* **2021**, *233*.

48. D'Anna, A.; Arrigo, R.; Frache, A. *J. Polym. Environ.* **2022**, *30*.

49. Casamento, F.; D'Anna, A.; Arrigo, R.; Frache, A. *J. Appl. Polym. Sci.* **2021**, *138*.

50. Verma, P.; Verma, M.; Gupta, A.; Chauhan, S. S.; Malik, R. S.; Choudhary, V. *Polym. Test.* **2016**, *55*.

51. Roman, C.; García-Morales, M.; Gupta, J.; McNally, T. *Polymer (Guildf).* **2017**, *118*.

52. Yetgin, S. H. *J. Mater. Res. Technol.* **2019**, *8*.

53. Inoya, H.; Wei Leong, Y.; Klinklai, W.; Thumsorn, S.; Makata, Y.; Hamada, H. *J. Appl. Polym. Sci.* **2012**, *124*.

54. Marotta, A.; Causa, A.; Salzano de Luna, M.; Ambrogi, V.; Filippone, G. *Polymers (Basel).* **2022**, *14*.

55. Sobkowicz, M. J.; Dorgan, J. R.; Gneshin, K. W.; Herring, A. M.; McKinnon, J. T. *J.*

Polym. Environ. **2008**, *16*.